Geotechnical Engineering in the XXI Century: Lessons learned and future challenges
N.P. López-Acosta et al. (Eds.)

doi:10.3233/STAL190140

Effects of Detailing on the Behavior of Helical Pile-to-Foundation Connections

Sundar CHILUWAL[a,1] and Serhan GUNER[a]
[a]*Department of Civil and Environmental Engineering, University of Toledo, OH, USA*

Abstract. Helical piles present a significant potential to create resilient, durable, and faster-to-construct foundations while ensuring a long-term and maintenance-free service life. To achieve their full potential, it is imperative that helical pile anchorages (i.e., pile-to-foundation connections) perform well without resulting in any cracking to the surrounding concrete. However, there is a lack of research and design guidelines on how to design resilient connections, especially for load conditions that create net uplift and cyclic loads. The objective of this study is to advance the current understanding and quantify the influences of anchorage bracket embedment depth, longitudinal reinforcement (ρ_x) percentage, shear span-to-depth (a/d) ratio, and the loading conditions on the load, deformation, cracking, and failure behavior of concrete foundations. For this purpose, 81 high-fidelity nonlinear finite element simulations of a pile cap strip are performed under monotonic tension, monotonic compression, and reversed-cyclic loads. The results indicate that the anchorage response may govern the response of the entire foundation system. Connection brackets with low embedment depths have been found to significantly reduce the load capacity of the foundation system, with a failure mode involving extensive anchorage zone cracking. The results also indicate that high ρ_x percentages and low a/d ratios should be used, along with higher embedment depths, in order to maximize the load resistance and prevent anchorage cracks for the load conditions involving tensile uplift loads. The research findings have applicability to both helical and micro piles given the fact that they both include similar anchorage conditions.

Keywords. Helical piles, helical pile anchorage, parameters, single bracket, longitudinal reinforcement, embedment depth, a/d ratio.

1. Introduction

Many structures are subjected to 'cyclic loads,' which involve sequential application of compression and tension loads due to events such as windstorms, earthquakes, or heavy vehicular traffic. Tall and light structures—such as telecommunication or transmission towers, wind turbines, and light-frame steel buildings—are particularly vulnerable to the tensile uplift components of cyclic loads. Helical piles (see Figure 1a) inherently possess high uplift resistances and thus present a significant potential to resilient, durable, and faster-to-construct foundations. To realize the full potential of helical piles, it is imperative that the helical pile anchorages (i.e., pile-to-foundation connections; see typically focus on the behavior of isolated helical piles without considering the influence of the concrete footing [1-8], while the structural studies focus on the footing response

[1] Corresponding Author, Sundar Chiluwal, Department of Civil and Environmental Engineering, The University of Toledo, 2801 W. Bancroft St., MS 307, Toledo, OH 43606, USA. Email: Sundar.Chiluwal@rockets.utoledo.edu.

[9-11]. Helical pile-to-footing connections are commonly designed in practice using 'rules of thumb' or simple bearing stress checks [e.g., 12]. Yet the failure of an Olympic-size swimming pool [13] and recent experimental studies [14] have shown this to be an oversight, by demonstrating that pile anchorages may govern the system response.

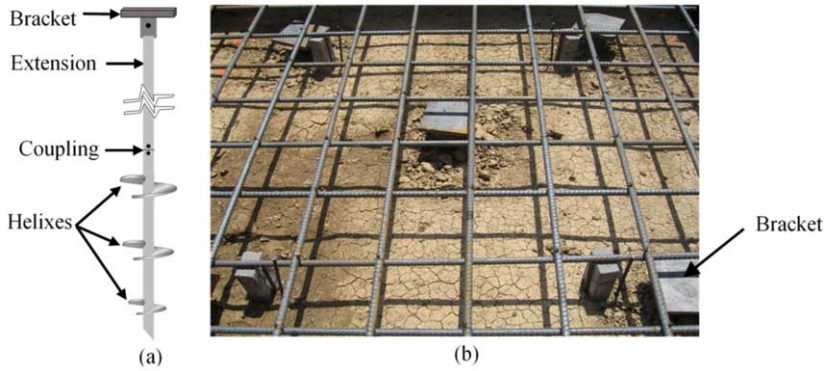

Figure 1. (a) A typical helical pile; (b) Anchorage of helical pile to a pile cap.

2. Objectives

The objective of this study is to quantify the influences of different pile anchorage configurations on the holistic behavior of pile caps—in terms of the load, deformation, cracking, and failure response—subjected to monotonic compression, monotonic tension, and reversed-cyclic load conditions.

3. Foundation system details

A foundation strip representative of commonly used foundation configurations (e.g., strip footings, grade beams, or a segment of pile caps) is designed, following the CRSI recommendations [15]. The strip is supported by two helical piles to create a one-way stress flow and better isolate the bracket response (see Figure 2).

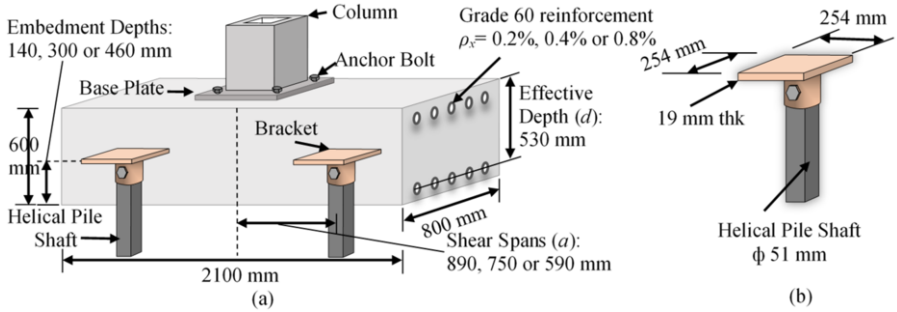

Figure 2. (a) Helical pile anchorage in the pile cap strip; (b) Details of single bracket.

Influencing parameters investigated include: three bracket embedment depths: 460 mm (top), 300 mm (middle), 140 mm (bottom); three longitudinal reinforcement percentages (ρ_x): minimum 0.2% (5-#5 rebars), 0.4% (7-#6 rebars) and 0.8% (10-#7 rebars); and three shear span-to-depth *a/d* ratios: 1.68, 1.42 and 1.11 (See Figure 2). When considering three loading conditions, 3^4=81 foundation systems are created.

4. Nonlinear finite element modeling

A two-dimensional, continuum-type, plane-stress element is used for the finite element modeling through the computer program VecTor2 [16]. The formulation is based on the Disturbed Stress Field Model [17], which is an extension of the Modified Compression Field Theory (MCFT) [18]. One sample numerical model created is shown in Figure 3a, where the concrete is modeled using a four-noded rectangular element with 8 degrees of freedom (see Figure 3b), and the longitudinal reinforcement is modelled using a two-noded truss bar (see Figure 3c) with 4 degrees of freedom. Table 1 shows the component properties in terms of their strengths and dimensions. VecTor2 incorporates several second-order material behaviors [19, 20] as listed in Table 2, including the cyclic response hysteresis (see Figures 4a and 4b) important for this study. A very fine mesh with a size of 20 mm x 20 mm is used where each helical pile is restrained with four hinges. A displacement-controlled analysis is employed which is advantageous when simulating the post-peak response, ductility, crack patterns, and failure modes. The results of the reversed-cyclic loading are divided into 'cyclic compression' and 'cyclic tension' to facilitate the comparison with the monotonic loading. *Cyclic tension* represents the uplift effects and *cyclic compression* represents the compressive effect (see Figure 5c).

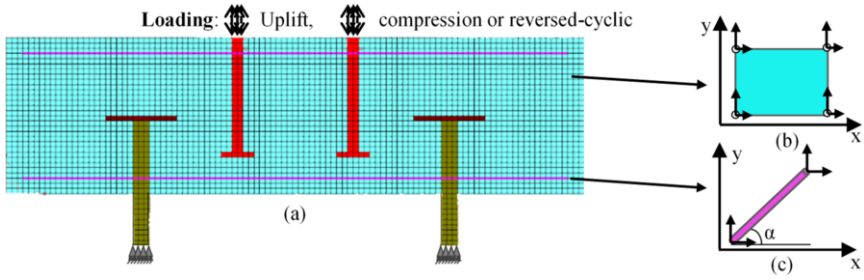

Figure 3. (a) Nonlinear FEM; (b) Plane stress rectangle elements; (c) Truss bar elements.

Table 1. Material properties.

Material	Description	Color	f_c (MPa)	fy (MPa)	Thickness (mm)
1	Concrete		20.7	-	800
2	Helical Pile			552	44
3	Bracket Plate		-	345	260
4	Anchor Bolt		-	724	57
5	Longitudinal reinforcement		-	414	-

Table 2. Concrete and reinforcement material models.

Material Behaviour	Default Model
Compressive Base Curve	Hognestad
Compression Post-Peak	Modified Park-Kent
Compression Softening	Vecchio 1992-:
Tension Stiffening	Modified Bentz 2003
Tension Softening	Linear
Confined Strength	Kupler/Richart
Concrete Dilation	Variable-Isotropic
Cracking criterion	Mohr-Coulomb (Stress)
Crack Width Check	Agg/5 Max crack width
Crack Slip	Walraven
Hysteretic Response	Bauchinger Effect (Seckin)
Dowel Action	Tassios (Crack Slip)
Buckling	Akkaya et al. 2019

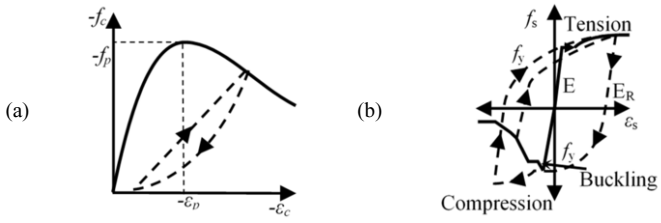

Figure 4. (a) Cyclic response of concrete; (b) Hysteretic response ductile steel reinforcement

5. Results

The simulation results show that the highest tensile resistance is obtained for the configurations involving higher embedment depths, higher ρ_x percentages, and lower *a/d* ratios. However, the compressive resistance of the foundation was found independent of the embedment depths. Figure 5 shows the load-displacement curves for a sample configuration involving an *a/d* ratio of 1.68 and ρ_x percentage of 0.4%.

Figure 6 shows the changes in load capacities in relation to the parameters investigated for all simulations. For the same color, the dashed and dotted lines lie above the solid lines in Figures 6a and 6b, which shows the increase of load capacity with the increase of embedment depth. The tensile load capacity is increased by an average of 29% when the embedment depth is changed from bottom to middle. In the same figures, the overlapped dashed and dotted lines confirm the similar load capacities for middle and top embedment depths.

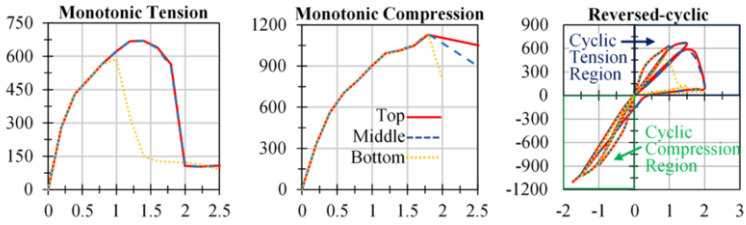

Figure 5. Load-displacement responses for *a/d* =1.68 and ρ_x =0.4%.

The tensile load capacity increases by an average of 23% and 19% when the ρ_x is increased from 0.2% to 0.4% and 0.4% to 0.8%, respectively. The tensile load capacity also increases by an average of 18% and 19% when the *a/d* ratio is decreased from 1.68 to 1.42 and 1.42 to 1.11, respectively. However, the tensile load capacity does not increase significantly for the bottom embedment depth even if the ρ_x percentage is increased or *a/d* ratio is reduced significantly. In Figures 6a and 6b, for example, the solid red, yellow and blue lines represent the bottom embedment depth; they all have smaller slopes as compared to other lines and are closer to each other. In addition, Figures 7a and 7b shows that the load capacity predictions for the bottom embedment depth are concentrated and do not increase as other embedment depths do.

The overlapping of the same colored lines in Figures 6c and 6d indicate that there is no significant influence of the embedment depth on the compressive resistance. The ρ_x percentage, on the other end, has a significant influence; the compressive capacity increases by an average of 24% and 26% when ρ_x is increased from 0.2% to 0.4% and 0.4% to 0.8%, respectively. Similarly, the compressive load capacity increases by an average of 25% when the *a/d* is decreased from 1.68 to 1.42 and 1.42 to 1.11.

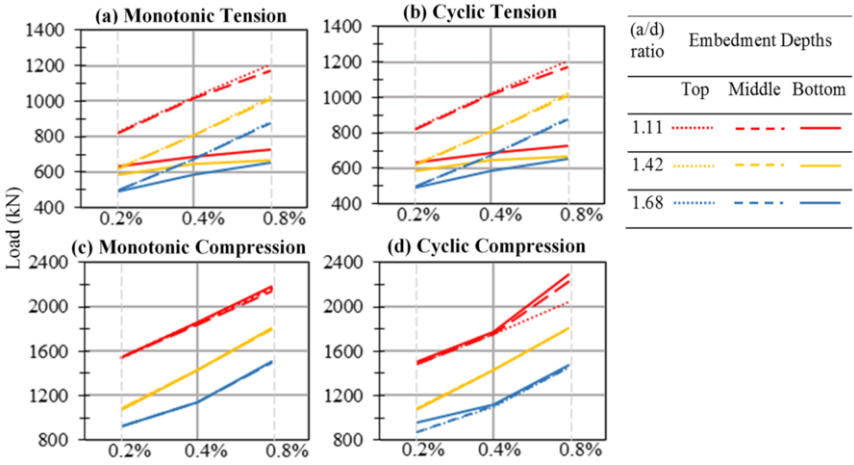

Figure 6. Effect of parameters on the load capacity subjected to different loading.

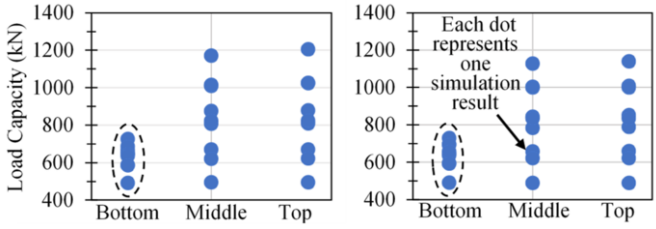

Figure 7. Summary of the ultimate load capacities from 54 simulation results for tension loads.

6. Failure modes and crack patterns

For monotonic tension loads, the simulation results indicate anchorage-zone concrete cracks for the bottom embedment depths (see Figure 8a), and local concrete cracking

along the top longitudinal reinforcement (see Figure 8b) for higher embedment depths. For monotonic compression loads, most failure modes are predicted as splitting of the concrete along the bottom reinforcement (see Figure 8c), and shear failures for the lowest *a/d* ratio (i.e., 1.11) with ρx of 0.4% or 0.8% (see Figure 8d). For reversed-cyclic loads, simulation results indicate anchorage-zone concrete cracks for the bottom embedment depths (see Figure 8e), and either local concrete cracking along the top and bottom longitudinal reinforcement (see Figure 8f) or shear cracks for a few cases in the lowest *a/d* (i.e., 1.11) and highest ρ_x (i.e., 0.8%) ratios (see Figure 8g) for higher embedment depths. Anchorage concrete cracks decrease the global load resistance of the foundation as compare to middle or top embedment depths. This could be attributed to insufficient bond resistance available in the helical shaft due to their shallow lengths.

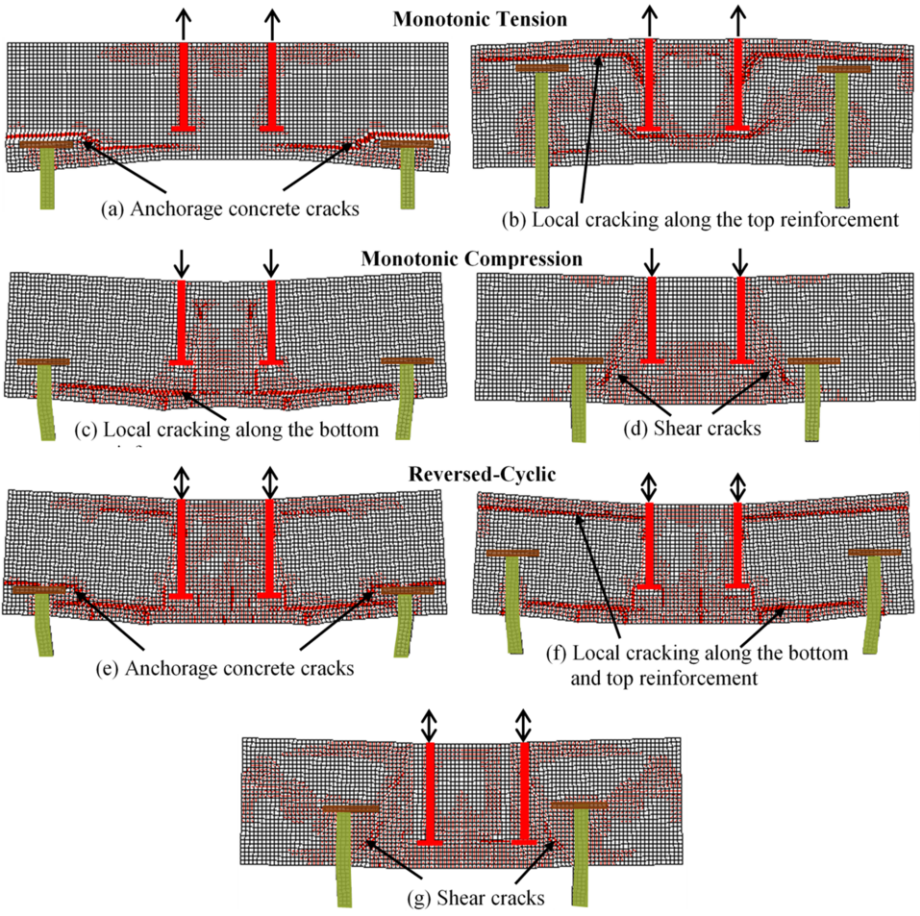

Figure 8. Failure modes and crack patterns.

7. Summary and conclusion

To fill the current knowledge gaps for helical pile anchorages, high-fidelity nonlinear finite element models were created (applicable to any general configuration of helical

piles and anchorages) to numerically investigate the effectiveness of commonly-used single bracket anchorages as well as the influence of embedment depths, longitudinal reinforcement (ρ_x) percentages, and shear span-to-depth (*a/d*) ratios. The results support the following conclusions.

Load Capacity for Monotonic and Cyclic Tension Loads

- The analysis indicates that 'embedment depth' is the most influential parameter, which also dictates the effectiveness of 'ρ_x percentage' and '*a/d* ratio' on the tensile load resistance.
- The tensile load capacity increases by an average of 29% when the 'embedment depth' is changed from bottom to middle.
- The analysis also reveals that there is no difference in tensile load resistance when the 'embedment depth' is either at the middle or top.
- The tensile load capacity increases by an average of 20% when ρ_x is increased from 0.2% to 0.4% or 0.4% to 0.8%.
- The tensile load capacity increases by an average of 19% when *a/d* ratio is decreased from 1.68 to 1.42 or 1.42 to 1.11.
- To maximize the tensile load resistance, high ρ_x percentages and low *a/d* ratios should be used, along with middle or top embedment depths.

Load Capacity for Monotonic and Cyclic Compression

- The 'ρ_x percentage' and '*a/d* ratio' influence the compressive load resistance while 'embedment depth' makes no influence.
- The compressive load capacity increases by an average of 25% when ρ_x is increased from 0.2% to 0.4% or 0.4% to 0.8%.
- The compressive load capacity increases by an average of 25% when the *a/d* ratio is decreased from 1.68 to 1.42 or 1.42 to 1.11.
- To maximize the compressive load resistance, high 'ρ_x percentages' and low '*a/d* ratios' should be used, regardless of the embedment depth.

Failure Modes

- Anchorage cracks (i.e., splitting concrete cracks around the brackets) for bottom embedment depths subjected to monotonic tension or reversed-cyclic loads are found to significantly decrease the global load resistance of helical pile foundation.

Acknowledgements

The authors would like to thank Helical Piles and Tiebacks Committee of the Deep Foundation Institution (DFI) for providing funding for this study.

References

[1] Elkasabgy, M. & El Naggar, M. H. (2013). Dynamic Response of Vertically Loaded Helical and Driven Steel Piles. *Canadian Geotechnical Journal*, *50*(5), 521–535. https://doi.org/10.1139/cgj-2011-0126

[2] Elsherbiny, Z. H., & El Naggar, M. H. (2013). Axial Compressive Capacity of Helical Piles from Field Tests and Numerical study. *Canadian Geotechnical Journal*, *50*(12), 1191–1203. https://doi.org/10.1139/cgj-2012-0487

[3] Prasad, Y. V. S. N., & Rao, S. N. (1996). Lateral Capacity of Helical Piles in Clays. *Journal of Geotechnical Engineering*, *122*(11). https://doi.org/10.1061/(asce)0733-9410(1996)122:11(938)

[4] Puri, V. K., Stephenson, R. W., Dziedzic, E., & Goen, L. (1984). Helical Anchor Piles under Lateral Loading. In and T. Langer, Mosley (Ed.), *Laterally Loaded Deep Foundations: Analysis and Performance*. American Society for Testing and Materials, 194–213. https://doi.org/10.1520/stp36822s

[5] Hambleton, J. P., Stanier, S. A., Gaudin, C., & Todeshkejoei, K. (2014). Analysis of Installation Forces for Helical Piles in Clay. *Australian Geomechanics Journal*, *49*(4), 73–80. Retrieved from https://www.researchgate.net/publication/271508701_Analysis_of_installation_forces_for_helical_pile sin_clay

[6] Vickars, R. A., & Clemence, S. P. (2000). Performance of Helical Piles with Grouted Shafts. In *New Technological and Design Developments in Deep Foundations*. Denver, CO: American Society of Civil Engineers, 327-341. https://doi.org/10.1061/40511(288)23

[7] Sakr, M., Naggar, M. H. El, & Nehdi, M. (2004). Load Transfer of Fibre-Reinforced Polymer (FRP) Composite Tapered Piles in Dense Sand. *Canadian Geotechnical Journal*, *41*(1), 70-88. https://doi.org/10.1139/t03-067

[8] El Sharnouby, M. M., & El Naggar, M. H. (2012). Axial Monotonic and Cyclic Performance of Fibre-Reinforced Polymer (FRP) – Steel Fibre–Reinforced Helical Pulldown Micropiles (FRP-RHPM). *Canadian Geotechnical Journal*, *49*(12), 1378–1392. https://doi.org/10.1139/cgj-2012-0009

[9] El Naggar, M. H., Youssef, M. A., & Ahmed, M. (2007). Monotonic and Cyclic Lateral Behaviour of Helical Pile Specialized Connectors. *Engineering Structures*, *29*(10), 2635–2640. https://doi.org/10.1016/j.engstruct.2007.01.018

[10] Youssef, M. A., Naggar, M. H. El, & Ahmed, M. (2006). Monotonic and Cyclic Load Behaviour of Helical Pile Connectors in the Vertical Direction. *Canadian Journal of Civil Engineering*, *18*(1996), 10–18. https://doi.org/10.1139/l05-074

[11] Guner, S., & Carrière, J. (2016). Analysis and Strengthening of Caisson Foundations for Uplift Loads. *Canadian Journal of Civil Engineering*, *43*(5), 411–419. Retrieved from http://www.utoledo.edu/engineering/faculty/serhan-guner/docs/JP6_Guner_Carriere_2016.pdf

[12] Pack, J. S. (2009). Design and Inspection Guide for Helical Piles and Helical Tension Anchors (4th ed.). Denver, CO: Intermountainhelicalpiers, Inc, 194 pp. Retrieved from http://www.intermountainhelicalpiers.com/downloads/DesignGuide4Rev2.pdf

[13] Labuda, T., Corley, G. W., & Murphy, M. (2013). Failure Investigation of a Helical Anchor Tie-Down System Supporting an Olympic Size Swimming Pool. In *Seventh International Conference on Case Histories in Geotechnical Engineering*. Chicago: Scholoars' Mine, Missouri University of Science and Technology. Retrieved from http://scholarsmine.mst.edu/cgi/viewcontent.cgi?article=3223&context=icchge

[14] Diab, M. A. M. (2015). Behavior of Helical Pile Connectors for New Foundations. Ph. D. Thesis, University of Western Ontario, London, Ontario, Canada, pp 638. Retrived from https://ir.lib.uwo.ca/cgi/viewcontent.cgi?article=4736&context=etd

[15] CRSI. (2015). Design Guide for Pile Caps (1st ed.). Schaumburg, IL: Concrete Reinforcing Steel Institute, pp 156. Retrieved from http://resources.crsi.org/resources/design-guide-for-pile-caps/

[16] Vecchio, F.J. (2019). VecTor2: Nonlinear Finite Element Analysis Software for Reinforced Concrete Structures [online]. Version 2.9. University of Toronto, ON, Canada.

[17] Vecchio, F.J. (2000). Disturbed Stress Field Model for Reinforced Concrete: Formulation. *Journal of Structural Engineering*, *126*(8): 1070–1077. https://doi.org/10.1061/(asce)0733-9445(2000)126:9(1070)

[18] Vecchio, F. J., & Collins, M. P. (1986). The Modified Compression Field Theory for Reinforced Concrete Elements Subject to Shear. *ACI Journal*, *83*(2), 219–231. https://doi.org/10.14359/10416

[19] Wong PS, Vecchio FJ, & Trommels H. (2013). VecTor2 and Formworks User's Manual. Technical Report, Department of Civil Engineering, University of Toronto, ON, Canada, pp 347. Retrived from http://www.vectoranalysisgroup.com/user_manuals/manual1.pdf

[20] Akkaya, Y., Guner, S., & Vecchio, F. J. (2019). A Constitutive Model for the Inelastic Buckling Behavior of Reinforcing Bars. *ACI Structural Journal, 116(3)*: 195-204. Retrieved from http://www.utoledo.edu/engineering/faculty/serhan-guner/docs/JP11_Akkaya_et_al_2019.pdf